Contribution of nuclei accelerated by gamma-ray pulsars to cosmic rays in the Galaxy

W. Bednarek[1] and R. J. Protheroe[2]

[1]Department of Experimental Physics, University of Łódź,
90-236 Łódź, ul. Pomorska 149/153, Poland.
[2]Department of Physics and Mathematical Physics,
The University of Adelaide, Adelaide, Australia 5005.

Abstract

We consider the galactic population of gamma-ray pulsars as possible sources of cosmic rays at and just above the "knee" in the observed cosmic ray spectrum at 10^{15}–10^{16} eV. We suggest that iron nuclei may be accelerated in the outer gaps of pulsars, and then suffer partial photo-disintegration in the non-thermal radiation fields of the outer gaps. As a result, protons, neutrons, and surviving heavier nuclei are injected into the expanding supernova remnant. We compute the spectra of nuclei escaping from supernova remnants into the interstellar medium, taking into account the observed population of radio pulsars.

Our calculations, which include a realistic model for acceleration and propagation of nuclei in pulsar magnetospheres and supernova remnants, predict that heavy nuclei accelerated directly by gamma-ray pulsars could contribute about 20% of the observed cosmic rays in the knee region. Such a contribution of heavy nuclei to the cosmic ray spectrum at the knee can significantly increase the average value of $\langle \ln A \rangle$ with increasing energy as is suggested by recent observations.

1   Introduction

The cosmic ray spectrum is usually described by a superposition of power laws with index ~ 2.7 below and ~ 3.2 above the so-called "knee" at a few 10^{15}eV. In the region of $10^{18} - 10^{19}$ eV the spectrum flattens, and has an index again close to 2.7. There are also suggestions that the shape of the spectrum in the knee region has a fine structure which may reflect acceleration of specific groups of nuclei, e.g helium, oxygen, and iron,

prominent in the Galactic abundances (see [1, 2] and references therein). Recent experimental results show that the cosmic ray composition changes through the knee region of the spectrum, becoming heavier with increasing energy [3, 4, 5]. For example, the CASA-MIA experiment measures the mass composition in the energy range $10^{14} - 10^{16}$ eV [3], and shows that above 10^{15} eV the iron group nuclei should dominate. The analysis of hybrid data from the High Resolution Fly's Eye prototype and the MIA muon array indicates that the mass composition becomes lighter again in the region $10^{17} - 10^{18}$ eV [6], and is proton dominated at around 10^{19} eV [7].

It is usually argued that cosmic rays with energies below 10^{14} eV are accelerated at shocks of expanding supernovae (see e.g. ref. [8]). It seems that the acceleration mechanism of the higher energy cosmic rays may be different, although supernova shocks of various types have also been proposed [9] and also lead to fine structure in the spectrum and composition in the knee region [10]. This idea is consistent with the recently observed variation in the composition of cosmic rays in the region $10^{15} - 10^{16}$eV mentioned above. However, it is uncertain what fraction of the cosmic rays above 10^{14} eV, are actually accelerated by supernova shocks, and so other mechanisms able to accelerate cosmic rays, particularly heavy nuclei, to energies above 10^{15}eV may be required. It has also been suggested that protons and heavy nuclei could be accelerated to such energies in pulsar winds [11, 12, 13, 14].

Nuclei can be also accelerated in pulsar magnetospheres as discussed by Cheng, Ho & Ruderman [15], Cheng & Chi [16] and Bednarek & Protheroe [17]. In our previous work [17, 18], we considered acceleration of iron nuclei in the magnetospheres of very young pulsars, and Crab-type pulsars, in the context of γ-ray and neutrino emission by supernova remnants. We found that, although the photo-disintegration process of iron nuclei during their acceleration and propagation through the neutron star magnetosphere is important, heavy nuclei would be injected into the medium of expanding supernova remnant. In the present paper we compute the possible contribution of nuclei injected by the galactic population of gamma-ray pulsars to the observed cosmic ray spectrum. We show that gamma-ray pulsars can contribute to the cosmic ray spectrum with energies above $\sim 10^{15}$ eV.

2 The pulsar spin evolution

Neutron stars are likely to be born with initial periods $P_0 \leq 10$ ms if we assume that the angular momentum of the pre-supernova star is conserved during the collapse. However, the initial angular momentum may be lost in the case of hot rapidly rotating neutron stars by emission of gravitational radiation due to the r-mode instability [19, 20, 21, 22]. As a result, the star would be left with a period of about 10 ms at about 1 year after its formation. After that, the period of the neutron star would change, mainly as a result of emission of magnetic dipole radiation with power given by

$$L_{em} = B^2 R_{NS}^6 \Omega^4 \sin^2 i / 6c^3, \tag{1}$$

where B is the surface magnetic field at the magnetic poles, R_{NS} is the radius of the neutron star, i is the angle between rotational and magnetic axes, and $\Omega = 2\pi/P$, where P is the period of the star. Also, gravitational radiation may be important for the case of stars having significant ellipticity k,

$$L_{\mathrm{gr}} = 32GI^2k^2\Omega^6/5c^5, \tag{2}$$

where G is the gravitational constant, I is the moment of inertia [23].

We have investigated the population of young pulsars observed with age $< 10^6$ years (about 100 pulsars) from the catalogue of Taylor, Manchester & Lyne [24] in order to estimate the neutron star ellipticity. By starting with an assumed initial period $P_0 = 10$ ms, perpendicular component of magnetic field $B\sin i$, and ellipticity k we may use Eqs. 1 and 2 giving the rate of loss of rotational kinetic by magnetic dipole radiation and gravitational radiation, respectively, to calculate the period P and period derivative $\dot{P}$ as a function of time since birth. For each of the young pulsars considered, and assuming standard values of I and R_{NS}, and the inferred value of $B\sin i$, we obtain the value of k such that P and $\dot{P}$ match those observed [25]. We note that the values of k obtained are rather insensitive to the assumed initial period for pulsars older than $\sim 10^3$ years. The results are plotted in Fig. 1, and show that a pulsar's ellipticity must be correlated with the perpendicular component of its surface magnetic field multiplied by its radius and divided by its moment of inertia. Since the theoretical radii and masses of neutron stars lie in a rather narrow range, we conclude that there exists a correlation between the ellipticity and the surface magnetic field for neutron stars. The correlation coefficient obtained is equal to ~ 0.65, which for 100 pulsars means that the correlation is highly significant. The inferred dependence of pulsar ellipticity on surface magnetic field can be well approximated by

$$\log k = -22.3 + 1.57\log B\sin i, \tag{3}$$

where B is in Gauss.

The above result suggests that the ellipticity of a pulsar may be due to the deformation of the shape of the neutron star by its strong interior magnetic field (see e.g. [26]). The prescription for pulsar spin evolution we apply in our present work is based on Eqs. 1–3. Note, however, that in the case of some specific pulsars, the difference between the result from Eq. 3 and estimates based on the known age of the pulsar is significant, e.g., in the case of the Crab pulsar for which the estimated ellipticity is $\sim 3 \times 10^{-4}$ [23]. In the case of the recently-discovered pulsar in the historical (AD 386) SNR G11.2-03, the standard formula [24] gives for the pulsar $B = 1.7 \times 10^{12}$ G, and using the historical age $t = 1612$ yr a pulsar initial period of 62 ms is found [27]. If gravitational radiation were included, the initial period could be much shorter. We find that for the same magnetic field, an ellipticity $k = 1.49 \times 10^{-3}$ would give an initial period of 10 ms for AD 386. This value of k, together with $B = 1.7 \times 10^{12}$ G, is consistent with the correlation described by Eq. 3 and seen in Fig. 1.

3

3   Acceleration of nuclei by young pulsars

Periodic emission of photons from radio to γ-ray energies gives direct evidence of the existence of electric potentials in neutron star magnetospheres which are able to accelerate particles to energies of at least ~ 100 GeV. To explain these observations, a number of models have been proposed including the polar gap model, the slot gap model, and the outer gap model (see e.g. Arons [28]). In the present paper, we concentrate on the outer gap model which is more attractive from the point of view of acceleration of nuclei by pulsars because it postulates induction of larger electric potentials in the pulsar's magnetosphere. The inner gap (polar cap) models (e.g. Ruderman & Sutherland [29], Harding & Muslinov [30]) predict that the electric potentials induced in the inner gaps are significantly lower (of the order of $\sim 10^{13}$ V), than expected in the outer gaps for pulsars with the same parameters. Nuclei accelerated through such potentials would not suffer efficient photo-disintegration in collision with thermal photons with a characteristic temperature $\sim 10^6$ K emitted by the polar cap or from the whole surface of a classical radio pulsar (only very young pulsars with ages of days to a month are sufficiently hot to photo-disintegrate Fe nuclei [18]). Hence, we neglect this stage of pre-acceleration of Fe nuclei during their passage through the inner gap. Moreover, the inner and outer gaps do not need to extend along these same magnetic field lines, and so they do not need to be physically connected.

Nuclei, most probably iron nuclei, can be stripped off the hot surface of a neutron star due to the strong electric fields and the bombardment by particles produced in the pulsar magnetosphere [29, 31]. This can occur where the magnetic and rotation axes are counter-aligned, and therefore where the co-rotation charge is positive above the poles, and can pull Fe nuclei from the surface. If one assumes that pulsars have random orientations of these axes, then Fe nuclei can be extracted from a significant fraction of pulsars, but if this is not the case then our results could be significantly affected.

These nuclei are then accelerated by the pulsar outer gap electric field to high energies. We assume that the process of extraction of iron nuclei from the pulsar surface occurs during the γ-ray emitting stage of the pulsar as the production of γ-rays in the outer gap requires efficient production of relativistic $e^{\pm}$ plasma, and this also heats the polar cap region. Chen & Ruderman [32] distinguish two types of gamma-ray pulsars, so called Crab-like (Crab-type) and Vela-like (Vela-type). Beyond the Vela-like death line the gap cannot close, and this prevents copious production of secondary $e^{\pm}$ pairs, and causes efficient production of gamma-ray photons to cease. However, electric potentials inside the outer gap remain, and the acceleration of primary particles is still possible. In more recent papers (Romani [33]; Zhang & Cheng [34]; Cheng & Zhang [35]) a third type of pulsar, so called Geminga-like pulsars, is distinguished. In these pulsars the production of secondary $e^{\pm}$ pairs inside the outer gap is sustained by the soft X-ray emission from the polar cap region. The death line for Geminga-like pulsars occurs when there is insufficient flux of thermal photons from the polar cap region of the pulsar. However, primary particles can be still accelerated inside the outer gap even after a pulsar has crossed the Geminga-like death line (only pair production stops). We expect that the injection of the Fe nuclei

from the region of the polar cap is related to the thermal radiation field produced by this region of the neutron star surface. The thermal radiation field drops significantly at a neutron star age $\sim 10^6$ yr (see Fig. 2 in Romani [33]). We estimate that at this age the pulsar stops injecting Fe nuclei into the magnetosphere.

3.1 Model for the electric field in the outer gap

During the γ-ray production stage of pulsars, three different types of outer gap can be distinguished, depending on the relative importance of different processes of γ-ray production: the Crab-type and Vela-type gaps (Cheng, Ho, Ruderman [15]), and the Geminga-type gap (Romani [33], Zhang & Cheng [34]). The separation between the Crab-type and the Vela-type outer gaps depends on the pulsar period and surface magnetic field, and is given by Eq. 25 of Chen & Ruderman [32]

$$P_{\mathrm{CV}} \approx 0.04 B_{12}^{2/5}, \tag{4}$$

where B_{12} is the pulsar surface magnetic field in 10^{12} G, and the period P_{CV} is in seconds. The maximum potential difference across different types of outer gap can be approximated by the simple formula (Cheng [36], private communication),

$$\Phi(B, P) \approx 6.6 \times 10^{12} f^2 B_{12} P^{-2} \text{ V}. \tag{5}$$

This formula gives the potential drop in outer gaps a factor of two lower than derived in original paper by Cheng, Ho & Ruderman [15], and is more consistent with the recent works on the outer gap model [37, 38]. However, we note that this simple formula may not match all observational data well because of uncertainties of viewing angle and inclination angle which are very important in determining the size of the outer gap. The parameter f is used to parametrize the gap voltage and power, and is defined by Cheng, Ho & Ruderman [15]

$$f \approx 82 B_{12}^{-13/20} P^{33/20}, \tag{6}$$

Formulae (5) and (6) give the potential difference $\sim 3 \times 10^{14}$ eV for the Crab pulsar. For Geminga-type gaps (Zhang & Cheng [34])

$$f \approx 5.5 B_{12}^{-4/7} P^{26/21}. \tag{7}$$

For Vela-type outer gaps a simple definition of the parameter f is not available. We assume that in this case the potential drop in the outer gap is equal to a constant fraction of the total potential drop in the outer gap given by Eq. (5) with $f^2 = 0.15$ for all periods (see [42]). The dependence of the potential difference across the outer gap as a function of the pulsar period is plotted in Fig. 2 for three different values of the surface magnetic field of the pulsar.

According to Cheng, Ho & Ruderman [15] the potential drop across the gap depends also on the position of injection into the outer gap field, z (z ranges between 0 and a), in relation to the maximum gap width a. Therefore, we assume that the potential drop for position z is given by (see definitions below eq. 3.10 in ref. [15])

$$\Phi(z) = 4\Phi(B, P)\frac{z}{a}[1 - \frac{z}{a}]. \tag{8}$$

3.2 Radiation field inside the outer gap

Iron nuclei accelerated in the outer gap potential can suffer significant photo-disintegration in collisions with photons produced inside the gap. We estimate the density of soft photons inside outer gaps of pulsars with a given period and magnetic field by scaling from the density of soft photons inside the outer gap of the Crab pulsar assuming the outer gap model. This density can be estimated from the observed pulsed flux of soft photons, assuming that the dimension of the outer gap is of the order of the light cylinder radius. Ho [39] has shown, by analyzing a sample of Crab-type pulsars with periods ~ 15 ms, that the luminosity of the photons produced in the gap does not change drastically for Crab-type outer gaps. Based on the results of Ho [39], we interpolate/extrapolate the density of photons in the present Crab outer gap for other periods. The γ-ray luminosity of pulsars scales as $\sim f^3$ times the total spin down pulsar luminosity [15], and so the γ-ray luminosity of the Crab type pulsars depends on the magnetic field as $\sim B^{1/20}$ (see Eq. 6), i.e. it is only very weakly dependent on B. Since energies of synchrotron photons are proportional to the magnetic field in the gap, then the photon density in Crab-type outer gaps should be inversely proportional to the pulsars' magnetic fields.

We note that the observations seem to suggest that the γ-ray luminosities of different types of pulsar are proportional to BP^{-2} (e.g. Fig. 7 in Arons [28]), although different models predict different dependencies of γ-ray luminosities on B and P [40]. However the above dependence should be considered with some caution because it interpolates between the Geminga pulsar (and PSR 1055-52) and the Vela pulsar (and its twin PSR 1706-44). The pulsar PSR 1951+32 deviates by an order of magnitude and the Crab pulsar by a factor of two, and if the distance to the Vela pulsar is ~ 250 pc but not ~ 500 pc [41], then Vela pulsar deviates by a factor of four from this dependence. Also, the distance to Geminga pulsar is not well known.

The density of soft photons in Vela-type outer gaps is obtained based on the observed change of the pulsed luminosity of the Vela type pulsars (e.g. [42]), and our estimate of f in the case of Vela-type pulsars, with the normalization to photon density in the Crab-type outer gap at the transition period given by Eq. (4). A good fit to the luminosity of the Vela-type pulsars is obtained if the density of photons in the outer gap drops with period as $\propto P^{-3}$. Therefore, we apply the following model for the soft photon density in Crab and Vela-type pulsars for different periods and surface magnetic fields

$$n_{\mathrm{ph}} \approx n_{\mathrm{ph}}^{\mathrm{Crab}} \begin{cases} \frac{P_{\mathrm{Crab}}B_{\mathrm{Crab}}}{PB}, & \text{the Crab-type;} \\ \frac{P_{\mathrm{Crab}}B_{\mathrm{Crab}}}{PB}\left(\frac{P_{\mathrm{CV}}}{P}\right)^3, & \text{the Vela-type,} \end{cases} \tag{9}$$

where $P_{\text{Crab}} = 0.033$ seconds, $B_{\text{Crab}} = 4 \times 10^{12}$ G and n_{ph}^{Crab} is the density of photons in the outer gap of the Crab pulsar at present [15](Cheng, Ho & Ruderman 1986).

The Geminga-type outer gap is determined by the thermal photons produced on the neutron star surface. This thermal radiation field for pulsars with ages corresponding to Geminga-type pulsars is too low to create a significant target for photo-disintegration of Fe nuclei. The epoch of gamma-ray emission of Geminga-type pulsars is determined by the temperature of the neutron star surface which, according to models of neutron star evolution, drops rapidly after $\sim 10^6$ years (see e.g. Fig. 2 in Romani [33]). Therefore, Geminga-type outer gaps should not be able to operate after $\sim 10^6$ years from the explosion of supernova. Here we assume that the process of extraction of Fe nuclei from the neutron star surface does not occur after this age because, as we noted above, it is probably caused by heating of the polar cap region by $e^{\pm}$ pairs created in the pulsar magnetosphere.

3.3 Number of nuclei accelerated in the outer gap

As in our previous paper [17], we assume that the number of Fe nuclei injected per unit time, $\dot{N}_{\text{Fe}}$, is simply related to the total power output of the pulsar $L_{\text{em}}(B, P)$ [43],

$$\dot{N}_{\text{Fe}} = \xi L_{\text{em}}(B, P)/Ze\Phi(B, P), \tag{10}$$

where ξ is a free parameter describing the fraction of the total power taken by relativistic nuclei accelerated in the outer gap, $Z = 26$ is the atomic number of Fe, and $\Phi(B, P)$ is defined by Eq. 5. The parameter ξ has to be always less than one since the power of accelerated Fe nuclei can never be greater than the spin-down power of the pulsar. The charge density estimated from Eq. 10 exceeds the 'classical' Goldreich-Julian charge density close to the polar caps $\rho = -(\Omega B/2\pi c)[1 - (\Omega r/c)^2 \sin^2 \theta]^{-1} \approx -\Omega B/2\pi c$, where the approximate formula is valid close to the surface where $\Omega r \sin \theta \ll c$. However, as noted by Goldreich & Julian [44] below their Eq. (8), the above formula is only valid in the co-rotation portion of the magnetosphere. If there is additional negative current onto the surface accompanying the charge injected from the surface in the form of Fe nuclei, then the above formula is not valid. Positive charge may flow onto the surface along the same magnetic lines as Fe nuclei, and could be produced somewhere in the pulsar magnetosphere, not necessary close to the pulsar's surface (e.g. possibly in the outer gap). Pair production just above the polar cap does not need to occur in this case.

3.4 Number of neutron stars with different parameters in the Galaxy

As discussed above, we assume that all pulsars are born with periods of about 10 ms, or that they reach this period soon after formation by emission of gravitational waves due to the r-mode instability. As we argued in Section 2, pulsars need to have a significant ellipticity k in order to reach their observed periods from a period at birth of 10 ms.

The distribution of the pulsar magnetic fields can be evaluated from observations, assuming that the surface magnetic field does not decay significantly with pulsar age. For example, Narayan [45] approximates the distribution of surface magnetic fields of pulsars at birth by

$$dN/d(\log B) \approx 0.065(10^{12}G/B) \text{ yr}^{-1}, \tag{11}$$

for $B > 2 \times 10^{12}$ G. We estimate the distribution of pulsars with surface magnetic fields below 2×10^{12} G based on the Fig. (13) in Narayan [45]. It is likely that this approximation underestimates the number of pulsars with relatively low magnetic fields because of observational selection effects. The above formula is normalized to a formation rate of pulsars in the Galaxy equal to 1 per 70 years.

4 Acceleration and propagation of nuclei from the neutron star surface

Nuclei extracted from the neutron star surface are accelerated and photo-disintegrated in the outer gap. Their disintegration products, and those which escape without any disintegration, are injected into the nebula and lose energy in collisions with matter ejected during the supernova explosion, and as a result of the expansion of nebula. All these processes are discussed below.

4.1 Propagation of nuclei through pulsar magnetospheres

The importance of photo-disintegration of nuclei with different mass numbers during propagation of nuclei in the radiation field of the outer gap is determined by the reciprocal mean free path, which we calculate using cross sections of Karakuła & Tkaczyk [46] (with improvements given in ref. [18]). The results of such a calculation for an outer gap with parameters applicable to the Crab pulsar are shown in Fig. 1 of Bednarek & Protheroe [17]. It is evident that multiple photo-disintegrations of primary Fe nuclei will occur for this pulsar. In our present calculations, the photo-disintegration of nuclei in the thermal radiation field emitted by the pulsar surface is neglected since it may be only important during a few days after creation of the pulsar when its surface temperature is of the order of 10^7 K [18], and consider only photodisintegration in the outer gap's non-thermal radiation field.

We simulate the photo-disintegration process of nuclei accelerated by pulsars using the evolution model, initial parameters of pulsars, the outer gap model for acceleration, and the radiation field discussed in Sections 2 and 3. Multiple photo-disintegrations occur only for pulsars with Crab and Vela-type outer gaps. We simulate the acceleration and propagation of iron nuclei in pulsar outer gaps in order to obtain the energy spectrum of neutrons and protons (extracted from Fe nuclei) and the spectra of escaping secondary nuclei. Note, however, that the fate of neutral particles (neutrons) and charged particles (protons and secondary nuclei) is different. The neutrons move ballistically through the

surroundings of the pulsar, and decay at distances determined by their Lorentz factors, and this can be inside or outside of the expanding envelope of the supernova. We compute the spectra of neutrons (and so protons from their decay) which decay inside and outside the Nebula as in Bednarek & Protheroe [17]. In the case of protons from neutrons decaying outside the nebula, we assume that all of them escape into the Galactic medium without being overtaken by the expanding nebula (we drop the second term in brackets in Eq. (5) in Bednarek & Protheroe [17] which represents the effects of protons from neutrons decaying outside the nebula being overtaken and trapped by the expanding nebula at some later time). This term can be neglected since the minimum diffusion distance of these protons, with Lorentz factor $\gamma_{\rm p} = 10^5$, in the Galactic magnetic field 5×10^{-6} G is comparable to the radius of nebula during its time of free expansion [17].

Protons and secondary nuclei injected into the Nebula are trapped by the magnetic field of the nebula, and suffer adiabatic and collisional energy losses during the time of expansion of the nebula. These effects are considered in the next subsection.

4.2 Interaction of nuclei with matter inside nebulae

Soon after the supernova explosion, when the nebula was relatively small, nearly all the energetic neutrons would be expected to decay outside the nebula. However, at early times we must take account of collisions with dense matter of the expanding nebula. The optical depth for neutrons moving ballistically through the envelope may be estimated from $\tau_{nH} \approx \sigma_{np} n_H r \approx 8.6 \times 10^{14} M_1 v_8^{-2} t^{-2}$, where $M = M_1 M_\odot$ is the mass ejected during the supernova explosion in units of solar masses, $r = vt$, $n_H = M/(4/3\pi r^3 m_p)$ is the number density of target nuclei, and $v = 10^8 v_8$ cm s^{-1} is the expansion velocity of the nebula. We note that $\tau_{nH} = 1$ at $t \approx 0.93 M_1^{1/2} v_8^{-1}$ yr.

Charged nuclei (protons, protons from decay of neutrons, and secondary nuclei) injected by the pulsar are captured by the nebula's magnetic field and interact with the dense material of the expanding supernova remnant. The optical depth for these nuclei depends on the time, t, of the injection of nuclei, and can be estimated from

$$\tau_{\rm Ap}(t) \approx 1.3 \times 10^{17} A^{2/3} M_1 v_8^{-3} t^{-2}. \tag{12}$$

Interactions of nuclei with matter inside the nebula become negligible when the optical depth becomes less than one. For the parameters derived for the Crab, $v_8 = 2$ and $M_1 = 3$, and the average value of the mass number of nuclei injected from the pulsar magnetospheres into the nebula $< A > \approx 48$, the nebula becomes transparent for nuclei at times $t > 3.6 \times 10^8 A^{1/3} M_1^{1/2} v_8^{-3/2} \approx 22$ years. Nuclei injected at earlier times should suffer significant fragmentation in collisions with the matter inside the nebula. We have simulated this process of fragmentation of nuclei injected by the pulsar applying the semi-empirical formulae for the cross sections for the fragmentation of nuclei of Silberberg & Tsao [47] with parameters given in their tables 1A,B,C,D. In our simulation, we assumed that in a single collision a nucleus fragments into two nuclei with different mass numbers.

Protons created during complete fragmentation of nuclei are considered as being captured by the magnetic field of the nebula. In contrast, neutrons which move ballistically

through the nebula have some chance of decaying inside or outside the nebula. These effects have been included in our simulation code. We consider the interactions of these secondary protons and neutrons with matter inside the nebula in the same way as for protons and neutrons from photo-disintegration of iron nuclei in the pulsar's magnetosphere.

4.3   Escape of nuclei from nebulae

We assume that nebulae expand during the free expansion phase with the velocity observed in the case of the Crab Nebula, i.e. 2000 km s^{-1}. When the amount of matter ejected during the supernova explosion becomes comparable to the amount of interstellar matter swept up by the nebula, then the nebula reaches the Sedov phase. The Sedov phase starts when the nebula reaches radius

$$R_{\mathrm{S}} = 6.8 \times 10^{18} (M_1/n)^{1/3} \text{ cm}, \tag{13}$$

and this occurs at time

$$t_{\mathrm{S}} = R_{\mathrm{S}}/v, \tag{14}$$

after the explosion. Here n is the density of the surrounding medium (cm^{-3}), and v is the expansion velocity of supernova during its phase of free expansion. For a supernova with an ejecta mass of $M_{\mathrm{SN}} = 3M_\odot$, a velocity of free expansion $v = 2000$ km s^{-1} as observed for the Crab Nebula, and a density of the interstellar medium $n = 0.3$ cm^{-3}, the Sedov phase should begin when the nebula reaches a radius of $R_{\mathrm{S}} \approx 4.8$ pc at about $t_{\mathrm{S}} \approx 2000$ years. This is only about twice as large as the present radius (and age) of the Crab Nebula. We assume the following approximation for the radius of a nebula at time t

$$R_{\mathrm{Neb}}(t) = \begin{cases} vt, & \text{if } t \leq t_{\mathrm{S}}; \\ vt_{\mathrm{S}}^{3/5} t^{2/5}, & \text{if } t > t_{\mathrm{S}}. \end{cases} \tag{15}$$

The magnetic field inside the nebula changes with time and depends on the distance from the center of the nebula, i.e. the pulsar. We estimate it applying the results of the Kennel & Coroniti [48] model, which gives the distribution of the magnetic field inside the nebula as a function of the parameter σ (the ratio of the magnetic energy flux to the particle energy flux at the location of the pulsar wind shock at radius R_{sh}). We estimate the magnetic field inside the nebula (in units of the magnetic field strength B_{sh} at the shock location) as a function of its radius based on the figs. 3 and 7 in Kennel & Coroniti [48]. For nebulae with $\sigma \gg 0.003$, the magnetic field drops significantly with the distance from the center of the nebula (fig. 3 in [48]), and can reach a value typical for the interstellar medium (5×10^{-6} G) at distance R_{B} which is less than the radius of the expanding nebula R_{Neb}, and so we assume that beyond radius R_{B}, the magnetic field is equal to 5×10^{-6} G.

The magnetic field at the shock, $B_{\rm sh}$, can be found from the dependence of the pulsar's magnetic field in the region of the inner magnetosphere ($B \propto R^{-3}$), and the pulsar wind zone ($B \propto R^{-1}$). It is given by

$$B_{\rm sh} \approx \sqrt{\sigma} B_{\rm s} \left(\frac{R_{\rm s}}{R_{\rm L}} \right)^3 \left(\frac{R_{\rm L}}{R_{\rm sh}} \right), \tag{16}$$

where $R_{\rm s}$ and $B_{\rm s}$ are the radius and the surface magnetic field of the pulsar, and $R_{\rm L} = cP/2\pi$ is the light cylinder radius of the pulsar. The value of σ is estimated for the Crab pulsar to be ~ 0.003 (e.g. Kennel & Coroniti [48]). However, it has recently been found that for the Vela pulsar the value of σ is rather close to 1 (Helfand et al. [49]). To our knowledge, there is no available information on σ for other plerions. Therefore, in order to fulfill observational constraints of these two pulsars, we assume that pulsars with periods lower than the period of the Crab pulsar have $\sigma \approx 0.003$ and pulsars older than the Vela pulsar have $\sigma \approx 1$. For pulsars having a rate of the rotational energy loss between that of the Crab and Vela pulsars, σ is obtained by linear interpolation between these two values.

The location of the wind shock, $R_{\rm sh}$, can be estimated from the comparison of the wind energy flux at the shock with the pressure of the outer nebula, which is determined by the supply of the magnetic energy to the nebula by the pulsar over its all lifetime (Rees & Gunn [50]). The location of the shock at an arbitrary time $t_{\rm p}$ after explosion of the supernova can be estimated from

$$\frac{L_{\rm em}(t_{\rm p})}{4\pi R_{\rm sh}^2 c} \approx \frac{\int_0^{t_{\rm p}} \sigma L_{\rm em}(t) dt}{\frac{4}{3}\pi R_{\rm Neb}^3}. \tag{17}$$

As an example, we show in Fig. 3 the characteristic radii in the nebula, $R_{\rm Neb}$, $R_{\rm sh}$, and $R_{\rm B}$, for the following parameters: $B_{\rm s} = 3 \times 10^{12}$ G, $k = 3 \times 10^{-4}$, $v = 2000$ km s^{-1}, $M_{\rm SN} = 3M_\odot$, and $n = 0.3$ cm^{-3}. The location of the shock, estimated from the above formula, is consistent with the observations of the shock in the Crab [48] and Vela [49] nebulae. For older nebulae $R_{\rm B}$ becomes less than $R_{\rm Neb}$, i.e. the magnetic field inside the outer regions of expanding nebula drops to 5×10^{-6} G.

Charged particles, nuclei and protons, injected into the nebula will diffuse, and finally escape from it into interstellar space. We assume that particles escape from a nebula at time $t_{\rm max}$ when the diffusion distance of particles injected at the time t becomes comparable to the radius of the nebula $R_{\rm Neb}$ at the time $t_{\rm max}$. In order to estimate this time at which they escape from the nebula, we compare the diffusion distance for nuclei with the mass number A and the Lorentz factor γ_A in the time dependent magnetic field inside an expanding nebula with radius given by Eq. 15. The distance diffused depends on the diffusion coefficient which we take to be

$$D = D_0 \rho^{1/3}, \tag{18}$$

as appropriate to a Kolmogorov spectrum of turbulence. Here, $\rho \approx E/eZ$ is the particle rigidity, and D_0 is normalized in such a way that $D = r_{\rm L} c/3$ when the Larmor radius,

$r_{\rm L}$, is equal to the radius of the remnant (largest scale) at time t (given by Eq. 15). This is a conservative assumption as it will give rise to the greatest trapping of nuclei in the nebula (and highest adiabatic losses) while being consistent with a Kolmogorov spectrum of turbulence. However, the precise form adopted for D has little effect on our results as most particles are released at $t_{\rm max}$. The diffusion distance is obtained by integration over time from the injection of nuclei at $t_{\rm inj}$ up to escape at $t_{\rm esc}$

$$r_{\rm dif} = \int_{t_{\rm inj}}^{t_{\rm esc}} \sqrt{\frac{3D}{2t'}} dt'. \tag{19}$$

Note that the diffusion coefficient depends on the age of the nebula, and this is included when integrating Eq. 19. For nuclei with sufficiently low energies, $t_{\rm max}$ may be shorter than $t_{\rm esc}$, and we then take $t_{\rm esc} = t_{\rm max}$. The adiabatic losses of particles inside nebula are considered up to the moment when the expansion velocity of the nebula during the Sedov phase, $v_{\rm exp} = v(t_{\rm S}/t)^{3/5}$, drops to a few tens km s^{-1} (i.e. to the characteristic velocities of the clouds in the interstellar medium). This happens at the age of $\sim 10^6$ yr. Note that at this age the magnetic field inside the nebula is larger than 5×10^{-6} G only at small region above the radius of the shock ($R_{\rm B} \approx 2R_{\rm sh}$, see Fig. 3).

Adiabatic and interaction energy losses of nuclei during the expansion of the nebula are included by estimating the Lorentz factor of nuclei at arbitrary time, t,

$$\gamma(t) = \gamma(t_{\rm inj}) \frac{t_{\rm inj} + t}{2t_{\rm inj} K^{\tau_{\rm Ap}(t)}}, \tag{20}$$

where K is the inelasticity coefficient, assumed equal to 0.5 for protons and neutrons. For nuclei with mass number A, we take the inelasticity coefficient to be $K \approx 0.5/A^{1/3}$ since the probability of a collision of a single nucleon within the energetic nucleus, with a proton of the remnant nebula is, on average, proportional to $(\sigma_{Ap}/A) \propto (A^{2/3}/A) \propto A^{-1/3}$.

5   Injection rate of nuclei into the Galaxy

Taking into account all of the effects discussed above, we compute the injection rate of nuclei of different mass numbers by the galactic population of pulsars into the interstellar medium, and this is given in Fig. 4(a). The spectrum shows two distinct maxima corresponding to heavy nuclei (dot-dot-dot-dash curve peaking at a few 10^{15}eV) and to protons (solid curve peaking at $\sim 10^{14}$eV). The contribution of medium mass nuclei is visible at energies between the proton maximum and the heavy nuclei maximum. The main contribution to the spectrum of nuclei below the high-energy peak is from Crab-type pulsars. This is clearly seen in Fig. 4(b) in which we present the contribution of pulsars having different types of outer gap to the total spectrum of nuclei injected into the Galaxy the from pulsars. The main contribution to the maximum at 3×10^6 GeV comes from Vela-type and Geminga-type pulsars. However the nuclei with the highest energies are injected by the Vela and Crab-type pulsars as expected from inspection of the electric potentials shown in Fig. 2.

6   Cosmic ray propagation

We assume that the radial distribution of the cosmic ray emission from gamma-ray pulsars follows the distribution of old neutron stars in the disk of the galaxy as given by Paczynski [51]

$$q(r)2\pi r\, dr = a_R \exp(-r/R_{\exp})R_{\exp}^{-2}2\pi r\, dr \tag{21}$$

with $a_R = 1.0683/2\pi$, $R_{\exp} = 4.5$ kpc, and r being the the distance from the centre of the Galaxy of radius $r_{\max} = 20$ kpc, and that they are uniformly distributed in a disk of thickness $2h_g$. For h_g we take an estimate of the scale height of pulsar birth locations, $h_g = 130$ pc [52], since random pulsar velocities ~ 200 km s^{-1} would not significantly increase the scale height for pulsars much younger than 10^6 y. Combining $q(r)$ with the calculated spectra of cosmic rays of atomic number Z, $Q_Z(E) = dN/dE/dt$ presented in Fig. 4(a), we obtain the spatial distribution of cosmic ray injection

$$\zeta(r, E) = q(r)Q_Z(E)/(2h_g). \tag{22}$$

We assume that at energies above 10^3 GeV we can reasonably neglect interactions and energy losses of cosmic ray nuclei, and that diffusion is the dominant process in shaping the observed cosmic ray spectrum. We consider two different models (Ptuskin et al [53]) for propagation of cosmic rays in the galaxy which are consistent with the observed secondary to primary ratios: (i) the minimal reacceleration model, and (ii) the standard diffusion model. We use the best-fitting parameters found by Ptuskin et al [53] for a halo half-thickness $h_h = 5$ kpc (we note here that the cosmic ray intensity at Earth obtained is rather insensitive to the value of h_g chosen provided that $h_g \ll h_h$). For the minimal reacceleration model, the diffusion coefficient used is

$$D = 3.8 \times 10^{29}(\rho/1\,\text{GV})^{1/3} \quad \text{cm}^2\text{s}^{-1} \tag{23}$$

where $\rho \approx E/Z$ is the particle rigidity. For the standard diffusion model, the diffusion coefficient used is

$$D = 3.0 \times 10^{28}(\rho/1\,\text{GV})^{0.54} \quad \text{cm}^2\text{s}^{-1}. \tag{24}$$

Assuming cylindrical geometry, we then use Eq. 3.22 of Berezinsky et al. [54], to calculate the cosmic ray density at Earth assumed to be in the Galactic plane 8 kpc from the centre of the Galaxy.

The spectra after propagation are plotted in Fig. 5 for the various species where they are compared with the world data set of observed cosmic ray intensity [55]. Fig. 5(a) and (b) show results for the two propagation models. The results are rather insensitive to the propagation model used, and this can be easily understood after inspecting the injection spectra in Fig. 4(a) and Eqs. 23–24. The peak at 10^5 GeV is due to protons with rigidity 10^5 GV, and the peak at $\sim 3 \times 10^6$ GeV is due to iron nuclei with rigidity 1.5×10^5 GV, approximately the same as the proton peak. Looking at Eqs. 23 and 24, we note that the diffusion coefficients for the two propagation models are equal at 1.8×10^5 GV, and this is within less than a factor of 2 of the rigidities of both the proton peak and the iron peak,

and so the two propagation models will give almost identical fluxes for the same pulsar injection spectrum. The propagated fluxes are interestingly close to those observed, with the region between 3×10^6 GeV and 2×10^7 GeV being about 20% of the observed flux.

7 Discussion and Conclusion

As can be seen in Fig. 5, we can expect fine structure in the spectrum in the region of the knee, as well as subtle composition changes. Our calculations were made assuming 100% efficiency of conversion of spin-down power into accelerated iron nuclei, i.e. $\xi = 1$ in Eq. 10. Other uncertainties entering our calculation relate the propagation of cosmic rays. The diffusion coefficients assumed were based on an analysis of lower energy cosmic ray data, and their extrapolation to higher rigidities may be questionable. This would increase our predicted flux if the actual diffusion coefficient were lower. Also, the pulsar formation rate is rather poorly known. With all these uncertainties, we feel justified is adopting $\xi \sim 1$ in order see whether injection of cosmic rays accelerated in pulsar outer gaps could be potentially interesting.

We shall next examine the composition in the knee region of the spectrum. The mass composition below $\sim 10^{15}$ eV is characterized by an average value of $< \ln A > \approx 1.2$ [3]. If we assume that this component of the spectrum extends to higher energies, and add to it the contribution of heavy nuclei (with average $A \approx 45$) as obtained for our pulsar acceleration model, this would change the average value of $< \ln A >$ to ~ 2.4 above the knee. Such a change in $< \ln A >$ has recently been reported for the CASA-MIA air shower array data [3].

Our calculations have assumed a steady-state production of pulsar-accelerated cosmic rays throughout the Galaxy with a smooth spatial distribution of sources following that inferred for pulsars. It neglects the effect of relatively nearby sources, such as any within 1 kpc releasing cosmic rays during the past 10^4 years which would enhance the pulsar contribution, and so the effects of pulsar acceleration on the cosmic ray composition could be even more dramatic. Finally, we conclude that pulsar-accelerated cosmic rays could make a significant contribution of heavy nuclei to the cosmic rays observed in the knee region, and that this would manifest itself as fine structure in the spectrum, and a heavy composition at 3×10^6–2×10^7 GeV.

Acknowledgements

References

[1] A.D. Erlykin, A.W. Wolfendale Astropart.Phys. 8 (1998) 265

[2] A.D. Erlykin, A.W. Wolfendale A&A 350 (1999) L1

[3] M.A.K. Glasmacher et al. Astropart.Phys. 12 (1999) 1

[4] F. Arqueros, J.A. Barrio, K. Bernlör, H. Bojahr, I. Calle et al., A&A 359 (2000) 682

[5] J.W. Fowler, L.F. Fortson, C.C.H. Jui et al. 2000 Astropart.Phys. in press, astro-ph/0003190

[6] T. Abu-Zayyad, K. Belov, D.J. Bird, J. Boyer, Z. Cao et al. 1999, astro-ph/9911144

[7] D.J. Bird et al. PRL 71 (1993) 3401

[8] E.G. Berezhko, H.J. Völk A&A 357 (2000) 283

[9] P.L. Biermann A&A 271 (1993) 649

[10] T. Stanev, P.L. Biermann, T.K. Gaisser A&A 274 (1993) 902

[11] J.P. Ostriker, J.E. Gunn ApJ 157 (1969) 1395

[12] S. Karakuła, J.L. Osborne, J. Wdowczyk J. Phys. A 7 (1974) 437

[13] Y.A. Gallant, J. Arons ApJ (1994) 435

[14] P. Blasi, R.I. Epstein, A.V. Olinto ApJ 533 (2000) L123

[15] K.S. Cheng, C. Ho, M. Ruderman ApJ 300 (1986) 500; ApJ 300 (1986) 525

[16] K.S. Cheng, X. Chi A&A 306 (1996) 326

[17] W. Bednarek, R.J. Protheroe PRL 79 (1997) 2616

[18] R.J. Protheroe, W. Bednarek, Q. Luo Astropart. Phys. 9 (1998) 1

[19] N. Andersson ApJ 502 (1998) 708

[20] N. Andersson, K. Kokkotas, B.F. Schutz ApJ 510 (1999) 846

[21] L. Lindblom, B.J. Owen, S.M. Morsink PRL 80 (1998) 4843

[22] B.J. Owen, L. Lindblom, C. Cutler, B.F. Schutz, A.Vecchio, N. Andersson Phys.Rev. D 58 (1998) 084020

[23] S.L. Shapiro, S.L. Teukolsky *Black Holes, White Dwarfs and Neutron Stars* (New York: Wiley, 1983)

[24] J.H. Taylor, R.N. Manchester, A.G. Lyne ApJS 88 (1993) 529

[25] A. Sierpowska, W. Bednarek Proc. IV INTEGRAL WORKSHOP (September 2000), submitted

[26] K. Konno, T. Obata, Y. Kojima A&A 352 (1999) 211

[27] K. Torii ApJ 523 (1999) L69

[28] J. Arons A&AS 120 (1996) 49

[29] M. Ruderman, P.G. Sutherland ApJ 196 (1975) 51

[30] A.K. Harding, A.G. Muslinov ApJ, 508 (1998) 328

[31] J. Arons, E.T. Scharlemann ApJ 231 (1979) 854

[32] K. Chen, M. Ruderman ApJ 402 (1993) 264

[33] R.W. Romani ApJ 470 (1996) 469

[34] L. Zhang, K.S. Cheng ApJ 487 (1997) 370

[35] K.S. Cheng, L. Zhang ApJ 498 (1998) 327

[36] K.S. Cheng (2000) private communication

[37] Hirotani, K., Shibata, S. MNRAS (1999) 308 54; 308 67

[38] K.S. Cheng, M. Ruderman, L. Zhang ApJ 537 (2000) 964

[39] C. Ho ApJ 342 (1989) 396

[40] A.K. Harding (2000) astro-ph/0012268

[41] A.N. Cha, K.R. Sembach, A.C. Danks ApJ 515 (1999) L25

[42] M. Ruderman, K.S. Cheng ApJ 335 (1988) 306

[43] R.N. Manchester, J.H. Taylor *Pulsars* (Freeman, San Francisco, 1977)

[44] P. Goldreich, W.H. Julian ApJ 157 (1969) 869

[45] R. Narayan ApJ 319 (1987) 162

[46] S. Karakuła, W. Tkaczyk Astropart. Phys. 1 (1993) 229

[47] R. Silberberg, C.H. Tsao ApJS 25 (1973) 315

[48] C.F. Kennel, F.V. Coroniti ApJ 283 (1984) 694

[49] D.J. Helfand, E.V. Gotthelf, J.P. Halpern ApJ (2000) in press, astro-ph/0007310

[50] M.J. Rees, J.E. Gunn MNRAS 167 (1974) 1

[51] B. Paczyński ApJ 348 (1990) 485

[52] J.M. Cordes, D.F. Chernoff, ApJ 505 (1998) 315

[53] V.S. Ptuskin, A. Lukasiak, F.C. Jones, W.R. Webber Proc. 26th ICRC (Salt Lake City) v.4 (1999) p.291

[54] V.S. Berezinskii et al. *Astrophysics of Cosmic Rays* (North-Holland; 1990)

[55] T.K. Gaisser, T. Stanev, review of cosmic ray data in Particle Data Group, Europhysics J. 3 (1998) 1
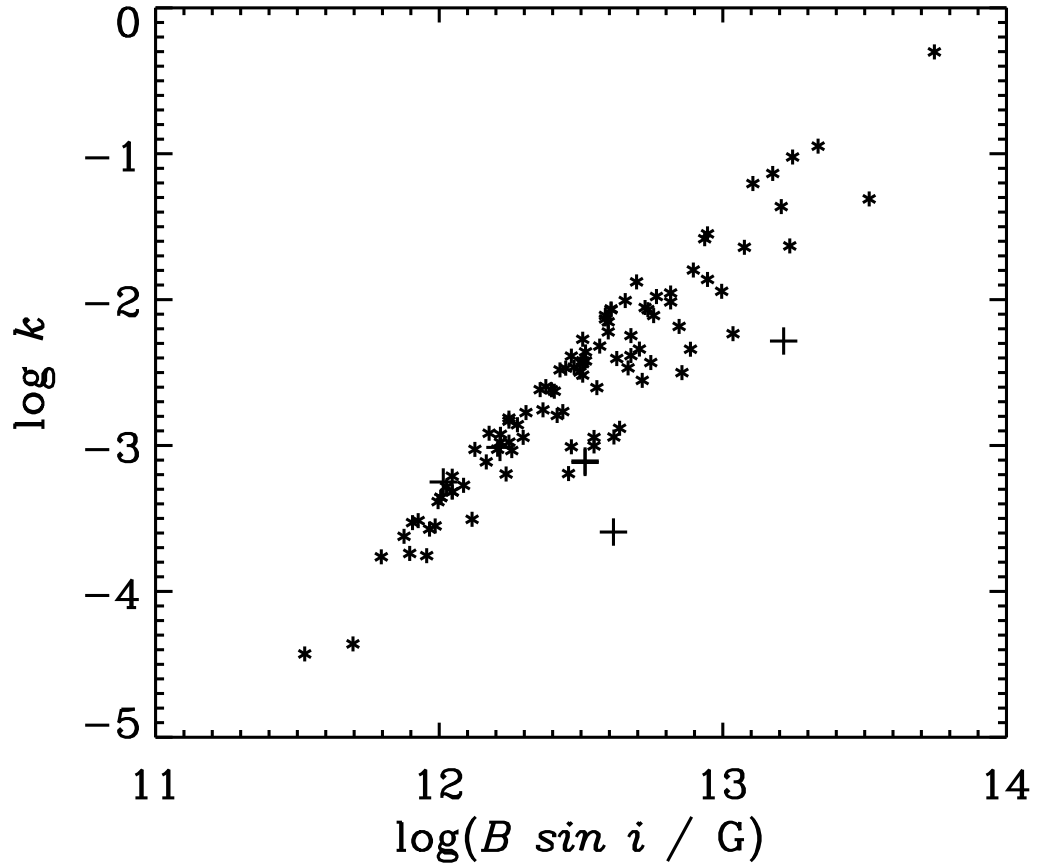
Figure 1: Correlation between the minimum values of ellipticity k of the pulsars with age $< 10^6$ years and their surface magnetic fields. The observed γ-ray pulsars are marked by crosses and other young pulsars are marked by stars. The initial periods of all pulsars have been fixed at $P_0 = 10$ ms.
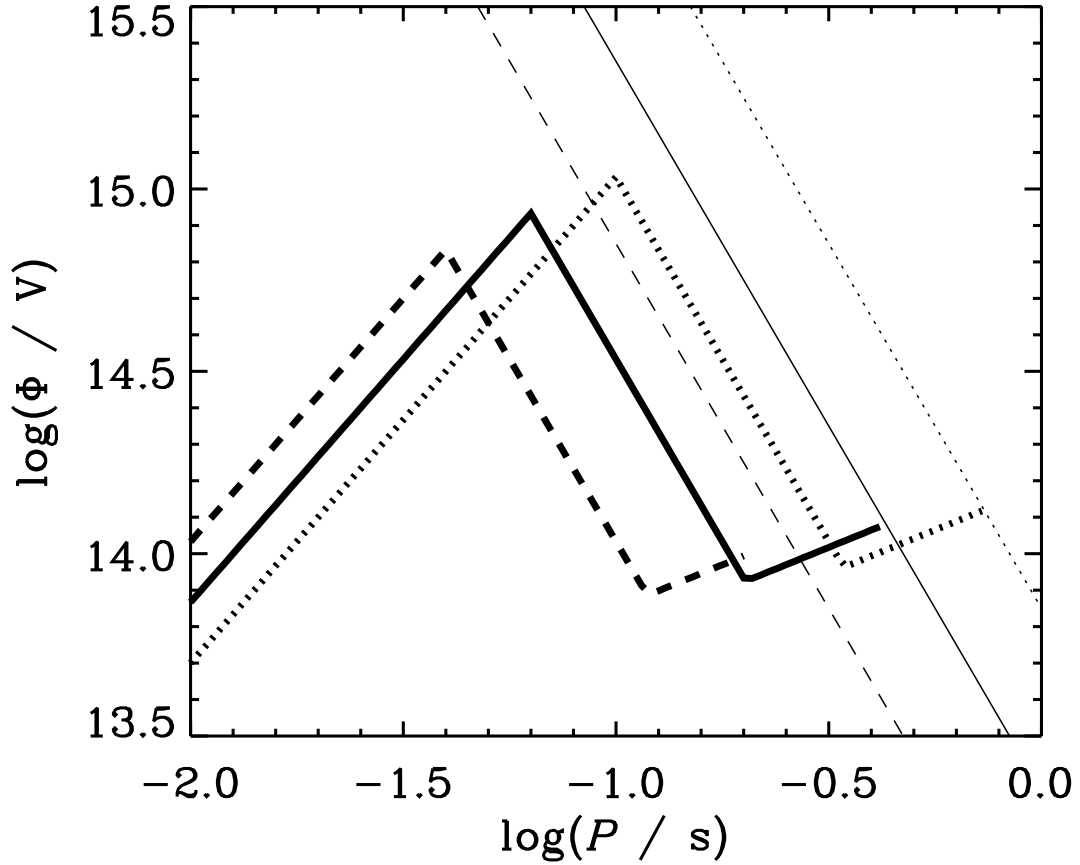
Figure 2: Dependence of the potential drop in the outer gap as a function of pulsar period for three values of surface magnetic field $B = 10^{12}$ G (dashed curve), $10^{12.5}$ G (full curve), and 10^{13} G (dotted curve). The corresponding thin lines show the maximum potential drop available across the region of the polar cap for three values of the magnetic field discussed above. For a given B value, Crab-type pulsars have the shortest periods, Vela-type pulsars have intermediate periods, and Geminga-type pulsars have the longest periods.
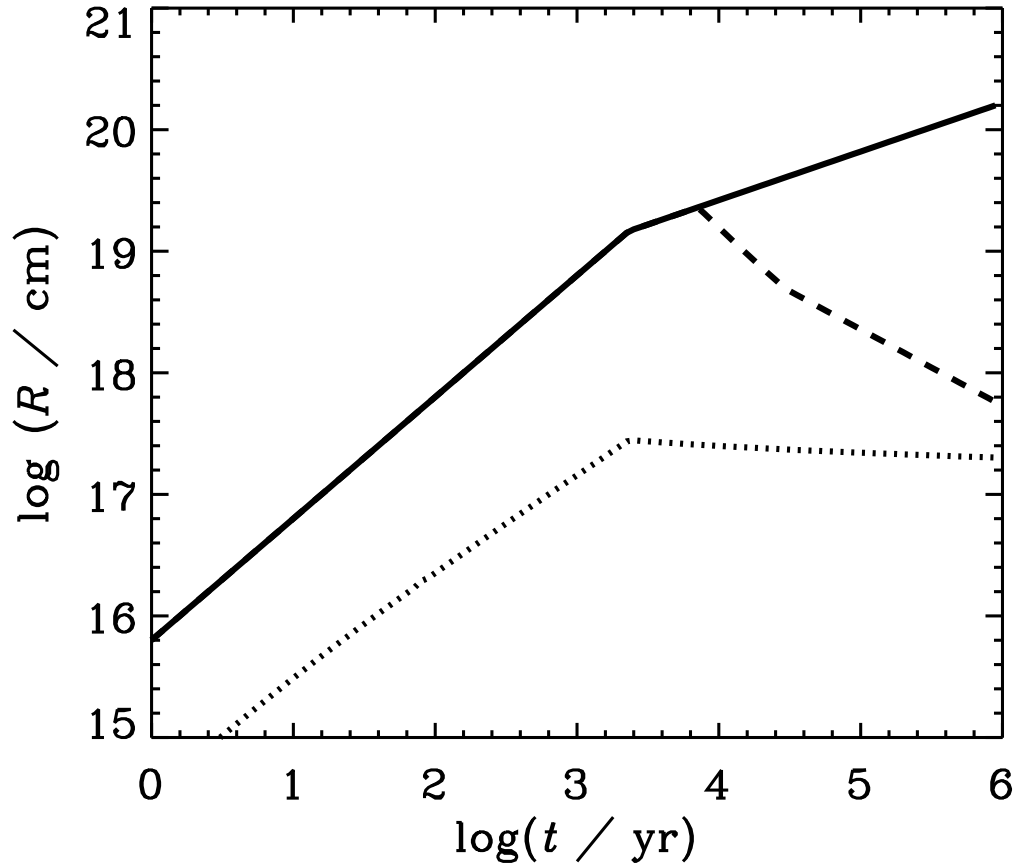
Figure 3: Radius of pulsar nebula (full line) as a function of age for a the pulsar with the parameters expected for the Crab pulsar and Nebula: surface magnetic field $B = 3 \times 10^{12}$, ellipticity $k \sim 3 \times 10^{-4}$ [23], initial expansion velocity $v = 2000$ km s^{-1}, mass of the supernova $M_{\mathrm{SN}} = 3M_{\odot}$, and density of the surounding medium $n = 0.3$ cm^{-3}. The dashed line shows the radius, R_{B}, above which the magnetic field drops to the value of the interstellar magnetic field (assumed 5×10^{-6} G), and the dotted line shows the radius of the inner shock, R_{sh}, produced by the interaction of the pulsar wind with the surounding nebula.
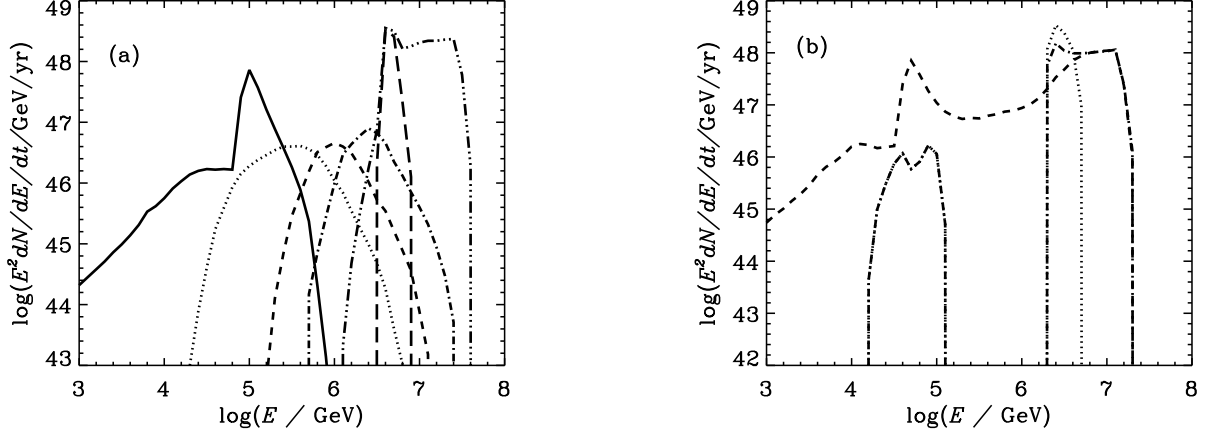
Figure 4: Differential spectrum of nuclei injected by pulsars into the interstellar medium, multiplied by the square of energy per nucleus. (a) Contribution of different groups of nuclei: solid curve – A=1; dotted curve – A=2–10; short dashed – A=11–20; dot-dashed – A=21–40; dot-dot-dot-dashed – A=41–56 (the contribution of A=56 is also shown separately as the long dashed curve). (b) Contribution of Crab (dashed curve), Vela (dot-dashed curve), and Geminga (dotted curve) type pulsars.
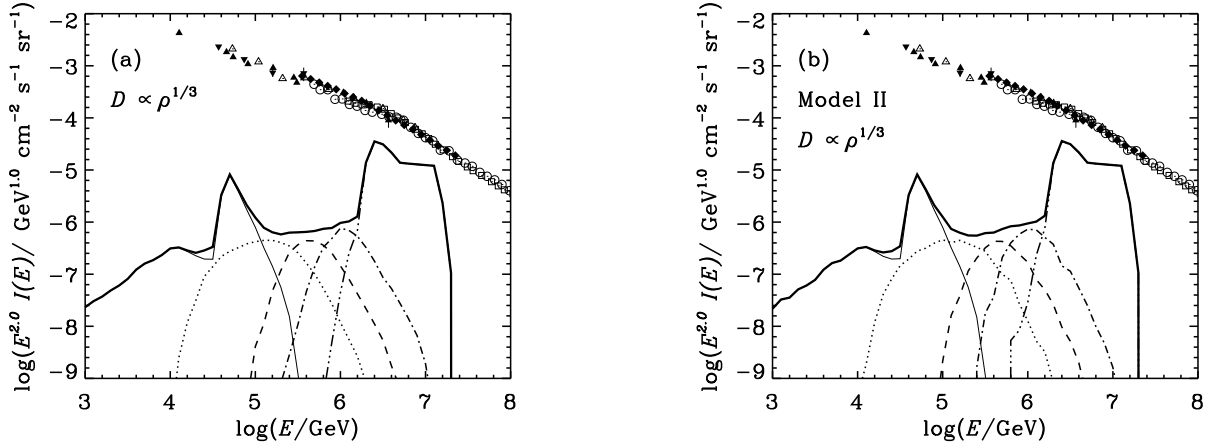

Figure 5: Differential spectrum of nuclei injected by gamma-ray pulsars after propagation as described in the text ($\xi = 1$). (a) $D \propto \rho^{1/3}$; (b) $D \propto \rho^{0.54}$. Key to curves: thick solid curve – total; thin solid curve – A=1; dotted curve – A=2–10; short dashed – A=11–20; dot-dashed – 21–40; dot-dot-dot-dashed – 41–56. The observed all-particle cosmic ray spectrum spectrum taken from ref. [55].